Proc. Natl. Acad. Sci. USA
Vol. 88, pp. 11540–11544, December 1991
Biophysics

Application of crystallographic and modeling methods in the design of purine nucleoside phosphorylase inhibitors

STEVEN E. EALICK*, Y. SUDHAKAR BABU†, CHARLES E. BUGG*†, MARK D. ERION‡, WAYNE C. GUIDA‡, JOHN A. MONTGOMERY†§, AND JOHN A. SECRIST III§

*University of Alabama, Birmingham, AL 35294; †BioCryst, Inc., Birmingham, AL 35205; ‡CIBA-Geigy Corp., Summit, NJ 07901; and §Southern Research Institute, Birmingham, AL 35255-5305

Communicated by Brian W. Matthews, July 8, 1991 (received for review February 6, 1991)

ABSTRACT **Competitive inhibitors of the salvage pathway enzyme purine-nucleoside phosphorylase (purine-nucleoside:orthophosphate ribosyltransferase, EC 2.4.2.1) have been designed by using the three-dimensional structure of the enzyme as determined by x-ray crystallography. The process was an iterative one that utilized interactive computer graphics, Monte Carlo-based conformational searching, energy minimization, and x-ray crystallography. The proposed compounds were synthesized and tested by an *in vitro* assay. Among the compounds designed and synthesized are the most potent competitive inhibitors of purine nucleoside phosphorylase thus far reported.**

The concept of drug design based on crystallographic and modeling methods has received much attention, yet few solid examples have appeared in the literature. Two notable exceptions are the reports by Erickson *et al.* (1) on the design of human immunodeficiency virus protease inhibitors and Appelt *et al.* (29) on the design of thymidylate synthase inhibitors. Advances in crystallography, computer graphics, and related fields have resulted in a dramatic increase in the number of macromolecular structure determinations while advances in computer hardware and computational methods have allowed the computational chemist to address more complex problems with higher accuracy (2, 3). Clearly, structural information combined with graphical methods for depicting the accessible volume, electrostatic potential, and active-site hydrophobicity aids drug design. Further enhancement in the quality of the "designed compounds" is expected from methods that can accurately evaluate the target molecule in terms of binding conformation, binding affinity, and binding-induced changes in protein conformation. We have developed Monte Carlo-based conformational search methods that, in combination with energy minimization, accurately predict the crystallographically observed ligand binding conformations for enzyme–inhibitor complexes. We now report the use of crystallographic and modeling methods for the design of competitive inhibitors of the enzyme purine nucleoside phosphorylase (PNP; purine nucleoside:orthophosphate ribosyltransferase, EC 2.4.2.1).¶

PNP as a Target for Drug Design. PNP catalyzes the reversible phosphorolysis of purine ribo- or 2′-deoxyribonucleosides to the purine and ribose- or 2-deoxyribose-α-1-phosphate. The enzyme has been isolated from both eukaryotic and prokaryotic organisms (4) and functions in the purine salvage pathway (5, 6). PNP isolated from human erythrocytes is specific for the 6-oxypurines and many of their analogs (7), while PNPs from other organisms vary in their specificity (8). The human enzyme is a trimer with identical subunits and a total molecular mass of ≈97 kDa (9, 10).

Interest in PNP as a drug target arises from its ability to rapidly metabolize purine nucleosides and from its role in the T-cell branch of the immune system. The chemotherapeutic potential of purine nucleoside analogs such as the 6-thiopurine 2′-deoxyribonucleosides (11) and 2′,3′-dideoxyinosine (12) may be severely compromised by PNP metabolism. Hence, a combination of a PNP inhibitor with these compounds may be highly efficacious. Administered alone, PNP inhibitors have potential therapeutic value since children lacking PNP activity exhibit severe T-cell immunodeficiency while maintaining normal B-cell function (13). This profile suggests utility for PNP inhibitors in the treatment of T-cell leukemias or lymphomas, in organ transplantation, and in T-cell-mediated autoimmune diseases such as rheumatoid arthritis and lupus. Despite the potential benefits of PNP inhibitors and despite the large number of PNP inhibitors that have been synthesized to date (4, 14), no compound has yet reached clinical trials. Although potencies for the best compounds have affinities 10–100 times higher than the natural substrate (K_m, ≈40 μM), it is expected that T-cell immunotoxicity will require very tight binding inhibitors (K_i, <10 nM) due to the high *in vivo* PNP activity and competition with substrate (15). Hence, we determined the structure of human PNP (Fig. 1) by x-ray crystallography (16) and have used these results in combination with computer-assisted molecular modeling to design highly potent inhibitors of this key enzyme.

Overall Strategy for Inhibitor Design. Once the structure of PNP was known, a scheme was used that involved both inhibition data and x-ray crystallography for evaluation of the synthesized compounds and a combination of these data and molecular modeling for the design of the next round of target molecules. A flow chart describing the overall strategy is shown in Fig. 2. Proposed compounds were screened by modeling the enzyme–inhibitor complex by using interactive computer graphics (17) and AMBER (18, 19) based molecular energetics. Monte Carlo/energy minimization techniques (20) were used to sample the conformational space available to potential inhibitors docked into the PNP active site. Qualitative evaluation of the enzyme–inhibitor complexes by molecular graphics and semiquantitative evaluation of the interaction energies between the inhibitors and the enzyme aided in prioritization for chemical synthesis. The resulting compounds were evaluated by determination of their IC_{50} values and by x-ray diffraction analysis using difference Fourier maps. The details of the modeling studies, organic syntheses, and x-ray diffraction experiments will be published elsewhere. The results of these analyses frequently led to proposed modifications of existing compounds or to the identification of new target compounds. Further analyses,

The publication costs of this article were defrayed in part by page charge payment. This article must therefore be hereby marked "*advertisement*" in accordance with 18 U.S.C. §1734 solely to indicate this fact.

Abbreviation: PNP, purine nucleoside phosphorylase.

¶The atomic coordinates and structure factors for PNP and PNP–guanine complex have been deposited in the Protein Data Bank, Chemistry Department, Brookhaven National Laboratory, Upton, NY 11973 (reference PNP3, PNP4) and will be released 1 year from the date of publication.

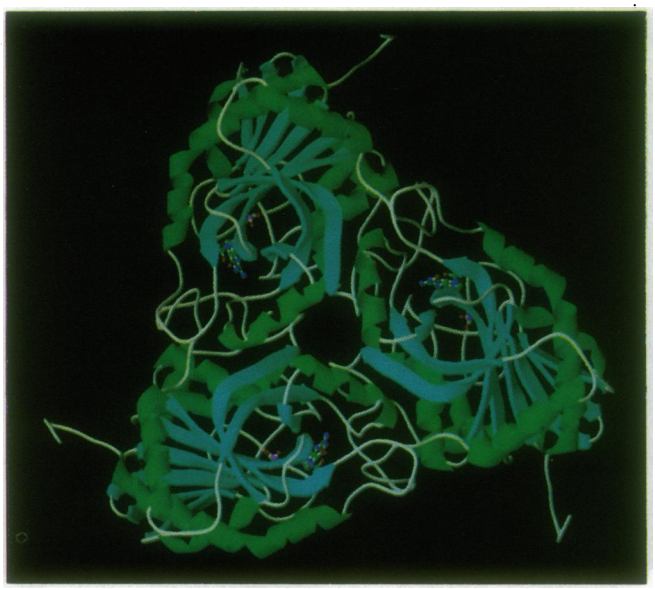

FIG. 1. Three-dimensional structure of human PNP. Each subunit in the trimer is represented by a ribbon that passes through the α-carbon positions. The molecule is viewed down the trimer axis. The ribbon is color-coded by secondary structure such that β-strands are green, α-helices are blue, and loops and turns are white. The substrates guanosine and phosphate are shown in the active site as ball and stick models.

such as K_i determinations and *in vivo* assays, were performed on the most potent compounds. Using this iterative process we were able to improve the potency of the best known membrane-permeable competitive PNP inhibitors by almost 2 orders of magnitude.

Description of the Active Site of PNP. The PNP trimer possesses three identical active sites near the interface between adjacent subunits. Each individual active site utilizes residues primarily from one subunit; however, participation of Phe-159 in the adjacent subunit is observed. The arrangement of key amino acids in the active site of PNP is shown in Fig. 3. The purine binding site is the most deeply buried and specificity for analogs of the 6-oxypurines is provided by Glu-201 and Lys-244, which form hydrogen bonds with purine atoms N(1)-H and O(6). The remainder of the purine binding site is largely hydrophobic, being composed of residues Ala-116, Phe-200, Val-217, Met-219, and Phe-159 of another subunit. These residues along with Thr-242 and Asn-243 form a cavity that accommodates a purine base.

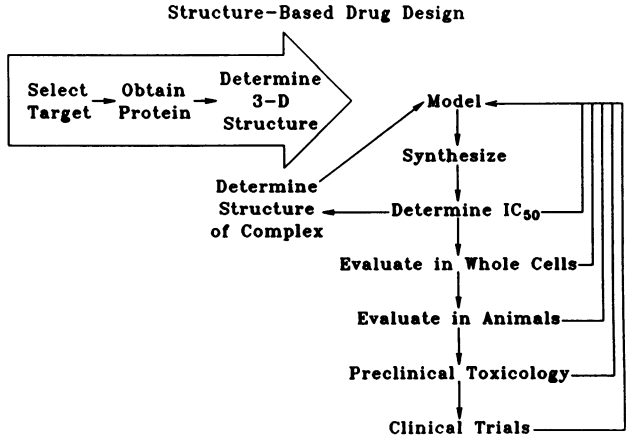

FIG. 2. Flowchart showing the overall strategy for the design of competitive inhibitors of purine nucleoside phosphorylase.

The phosphate binding site, composed of residues Ser-33, Arg-84, His-86, and Ser-220, is located near a glycine-rich loop (residues 32–37) with the phosphate positioned for nucleophilic attack at atom C(1′) of the nucleoside. The ribose binding site is largely hydrophobic and contains a hydrogen bonding group, Tyr-88, which interacts with the O(3′) position. The residue nearest O(2′) is Met-219 and the residue nearest O(5′) is His-86. One side of the ribose binding site contains several aromatic amino acids including Phe-159, Phe-200, His-86, and Tyr-88. This hydrophobic patch serves to orient the ribose to facilitate nucleophilic attack by phosphate and subsequent inversion at C(1′).

A Swinging Gate Controls Access to the Active Site. The initial electron density for PNP was weak and poorly defined near residues 241–260 (16), indicating high thermal motion for these residues. X-ray analysis of many complexes of PNP with substrates or inhibitors has now confirmed that these residues form a gate that opens during substrate binding to accommodate the substrate or a competitive inhibitor. The maximum movement after substrate or inhibitor binding occurs at His-257, which is displaced outward by several angstroms. The gate is anchored near the central β-sheet at one end and near the C-terminal helix at the other end. The gate movement is complex, apparently involving a helical transformation near residues 257–261. Consequently, initial inhibitor modeling attempts using the native PNP structure were far less successful than subsequent analyses using coordinates for the guanine–PNP complex.

Previously Known PNP Inhibitors. Prior to our studies, several PNP inhibitors had been reported with K_i values of 10^{-6}–10^{-7} including 8-aminoguanine (21), 9-benzyl-8-aminoguanine (22), and 5′-iodo-9-deazainosine (23). Acyclovir diphosphate (24) had a K_i value near 10^{-8} if assayed at 1 mM phosphate rather than the more frequently used value of 50 mM. During our studies, the synthesis of 8-amino-9-(2-thienylmethyl)guanine (K_i, 6.7×10^{-8} M) was reported (25). Complexes of these compounds bound to PNP, which were analyzed by x-ray crystallography, are illustrated in Fig. 4. The most important findings were the following: (*i*) 8-amino substituents enhance binding of guanines by forming hydrogen bonds with Thr-242 and possibly the carbonyl oxygen atom of Ala-116, (*ii*) 9-deaza analogs acquire potency through donation of a hydrogen bond to Asn-243, (*iii*) substitution by hydrophobic groups at the 9-position of a purine enhances binding through interaction with the hydrophobic region in the ribose binding site, (*iv*) acyclovir diphosphate is a multisubstrate inhibitor in which the acyclic spacer between N(9) of the purine and the phosphate is optimal for accommodating the two binding sites, and (*v*) additional binding affinity in acyclovir diphosphate may result from a hydrogen bond between the α-phosphate and Tyr-88 and from the interaction of the ethylene spacer and the hydrophobic region. Based on these results, a number of compounds were proposed that incorporated these and other features predicted to enhance inhibitor binding.

The Hydrophobic Patch in the Ribose Pocket Contributes to Tight Binding Inhibitors. An initial series of compounds synthesized in this program exploited the hydrophobic region in the ribose binding site. A number of 9-substituted 9-deazapurine analogs were prepared with various aromatic, heteroaromatic, and cyclic aliphatic substituents. Crystallographic data showed that generally the planes of the aromatic rings tend to orient in a reproducible conformation. The aromatic groups optimize their interaction with Phe-159 and Phe-200 resulting in the classic herringbone arrangement reported in a variety of aromatic systems (26). In some cases, ring substitution resulted in displacement of the molecular centroid; however, the ring tilt relative to Phe-159 and Phe-200 remained relatively constant. The optimum spacer

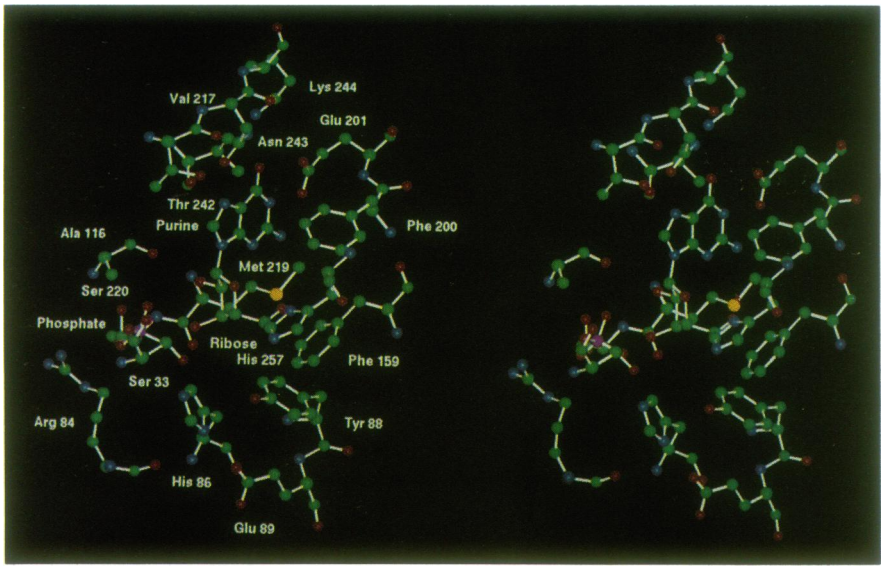

FIG. 3. Ball and stick model of key residues in the active site of PNP. Color coding is by atom type with carbon atoms green, oxygen atoms red, and nitrogen atoms blue. Models of guanosine and phosphate that were determined from x-ray crystallographic studies are also shown.

between the purine base and the aromatic substituent appears to be a single methylene group.

Inhibitors with cyclic aliphatic substituents at N(9) were as potent as the aromatic analogs discussed above with the aliphatic substituents occupying the same general volume as the aromatic groups (Table 1). As with the aromatic series, the optimum spacer was one carbon atom. X-ray analysis of the PNP complex of 9-cyclohexyl-9-deazaguanine and the complex of 9-cyclohexylmethyl-9-deazaguanine showed the surprising result that the two cyclohexyl groups occupy approximately the same volume and the 9-deazapurine of the cyclohexyl analog is shifted in order to accommodate the nonoptimal fit to the active site.

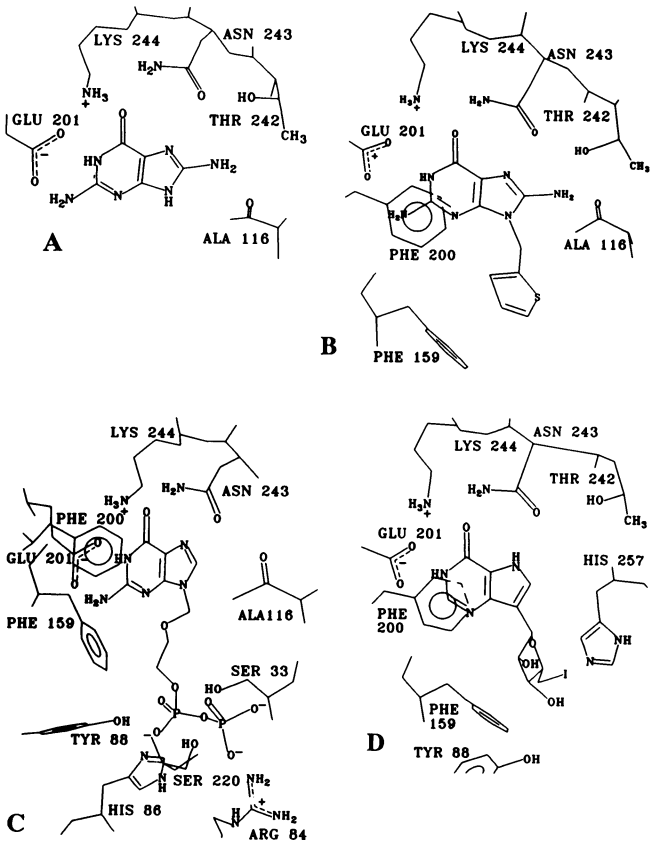

FIG. 4. Line drawings of representative inhibitors in the active site of PNP. The inhibitors are 8-aminoguanine (*A*), 8-amino-9-(2-thienylmethyl)guanine (*B*), acyclovir-diphosphate (*C*), and 5′-iodo-9-deazainosine (*D*). The models were prepared from analysis of difference Fourier maps using 3.2 Å resolution data and calculated phases.

Inhibitor Potency Is Dependent on Phosphate Concentration for a Wide Variety of Compounds. Previously, Tuttle and Krenitsky (24) established that the K_i value for acyclovir diphosphate was larger at 50 mM phosphate (standard assay conditions) than at 1 mM phosphate (cellular conditions) (27). This result can be explained by competition between the distal phosphate group and inorganic phosphate for the phosphate binding site. During our crystallographic analysis of certain PNP–inhibitor complexes, we discovered significant displacements of the inhibitors in the active site that appeared to result from close contacts between the inhibitor and a sulfate ion that occupies the phosphate binding site.

Table 1. Inhibition data for selected PNP inhibitors by increasing IC_{50} value

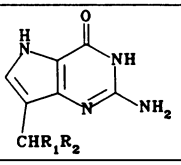

R_1*	R_2	IC_{50}, μM: 50 mM phosphate†	IC_{50}, μM: 1 mM phosphate‡	Ratio§
(*S*)-3-Chlorophenyl	CH_2CO_2H	0.031	0.0059	5.3
3-Chlorophenyl	CH_2CN	1.8	0.010	180
2-Tetrahydrothienyl	H	0.22	0.011	20
3,4-Dichlorophenyl	H	0.25	0.012	21
3-Thienyl	H	0.08	0.020	4.0
3-Trifluoromethylcyclohexyl	H	0.74	0.020	37
Cyclopentyl	H	1.8	0.029	62
Cycloheptyl	H	0.86	0.030	29
Pyridin-3-yl	H	0.20	0.030	7.3
2-(Phosphonoethyl)phenyl¶	H	0.45	0.035	13
Cyclohexyl	H	2.0	0.043	47
2-Furanyl	H	0.31	0.085	3.6
(*R*)-3-Chlorophenyl	CH_2CO_2H	0.90	0.16	5.6
2-Phosphonopropoxyphenyl¶	H	42	1.0	42

*Compounds with R_2 not equal to H are racemic mixtures unless the *R* or *S* isomer is designated.
†Calf spleen PNP assayed in 50 mM phosphate buffer.
‡Calf spleen PNP assayed in 1 mM phosphate buffer.
§IC_{50} at 50 mM phosphate divided by IC_{50} at 1 mM phosphate.
¶Guanine base.

Therefore, we assayed these and other PNP inhibitors at both 1 mM and 50 mM phosphate. These results, summarized in Table 1, show that the IC_{50}(50 mM) is equal to or larger than the IC_{50}(1 mM), in some cases by as much as 100-fold. The ratio and the dimension of the 9-substituent show some correlation. Some compounds, such as 8-aminoguanosine and 8-amino-9-(2-thienylmethyl)guanine, show no difference. In the case of nucleosides, the result may be due to a hydrogen bond between the phosphate and O(3'). Since the concentration of phosphate in intact cells is ≈1 mM, we routinely used this assay condition for all PNP inhibitors.

8-Amino-9-deazaguanine Analogs Are Poor Inhibitors. Both 8-aminoguanine analogs and 9-deazaguanine analogs are good inhibitors of PNP; however, the first 8-amino-9-deazapurine analog prepared was a relatively poor PNP inhibitor. To explain this poor binding, we undertook crystallographic analysis of PNP complexes with four compounds having a 9-thienylmethyl substituent but with the bases being guanine, 8-aminoguanine, 9-deazaguanine, and 8-amino-9-deazaguanine. The results of the x-ray analysis are summarized in Fig. 5. These data showed one binding mode for compounds that accept a hydrogen bond at N(7) and another for compounds that have a hydrogen bond donor at N(7). In both types of binding, a hydrogen bond is formed between N(7) and Asn-243. The 8-aminoguanine analogs make use of the Thr-242 side chain to form an additional hydrogen bond and to improve binding affinity. When N(7) has an attached hydrogen atom, Asn-243 undergoes a shift that is clearly seen in difference Fourier maps and is probably caused by the formation of the highly favorable N(7)-H···O hydrogen bond. A concomitant shift by Thr-242 results in its inability to hydrogen bond to 8-amino substituents. Furthermore, the overall conformational change causes the γ-carbon of Thr-242 to approach the 8-position of the purine, thereby generating a hydrophobic environment for the 8-amino group and causing a decrease in binding affinity. Table 2 lists IC_{50} values for several PNP inhibitors, which exhibit this striking phenomenon.

Branching at the Benzylic Carbon Atom Allows for Optimum Binding of Multisubstrate Inhibitors. To take full advantage of the binding properties of the enzyme active site, it is necessary to design compounds that bind to all three subsites. Acyclovir diphosphate, although not membrane permeable and subject

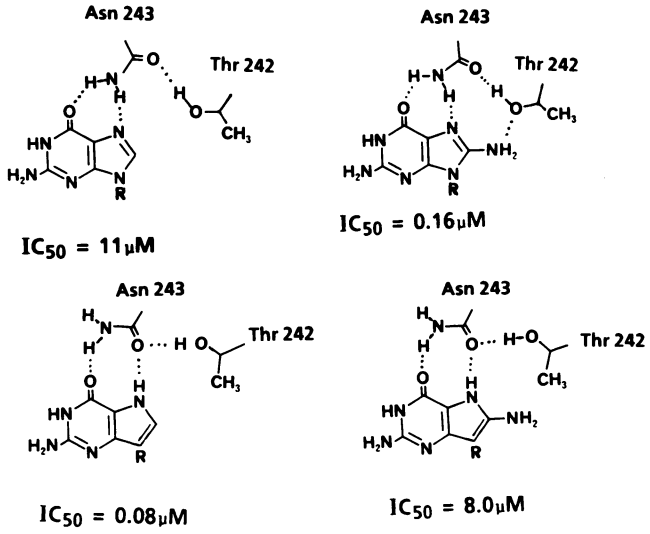

FIG. 5. Comparison of the effects of 8-amino and 9-deaza modifications of purine analogs. The R group is 2-thienylmethyl in the purine example and 3-thienylmethyl in the 9-deazapurine example. Proposed hydrogen bonds, shown as dotted lines, are derived from the analysis of difference Fourier maps. The IC_{50} values are taken from Table 2 at 50 mM phosphate.

Table 2. Effects of 8-amino substitution

9-substituent	IC_{50}, μM			
	G	8-AG	9-DG	8-A-9-DG
2-Thienylmethyl	11*	0.16*	0.14	—
3-Thienylmethyl	—	0.085*	0.08	8.0
Benzyl	—	0.47*	0.23	7.7
Cyclohexylmethyl	—	—	2.2	150
3-Methyl-2-thienyl methyl	48*	4*	—	—
2-Furanylmethyl	18*	0.25*	0.31	—

Calf spleen PNP was assayed in 50 mM phosphate buffer. G, guanine; 8-AG, 8-aminoguanine; 9-DG, 9-deazaguanine; 8-A-9-DG, 8-amino-9-deazaguanine.
*Human erythrocytic PNP assayed in 50 mM phosphate buffer (28).

to extracellular metabolism, is a good example. Our results suggest that an ideal PNP inhibitor in the 9-deazapurine series would contain a bulky hydrophobic group and a substituent with affinity for the phosphate site interlinked by spacers with optimum lengths. Crystallographic and modeling studies suggested a single atom as the optimal spacer between the purine base and hydrophobic group, while modeling studies using coordinates from the native enzyme suggested that a two- to four-atom spacer should link the hydrophobic group to a group having affinity for the phosphate binding site. Such a compound (structure 1) with a four-atom spacer from the ortho position of a benzyl group to a phosphonate group was a surprisingly poor PNP inhibitor.

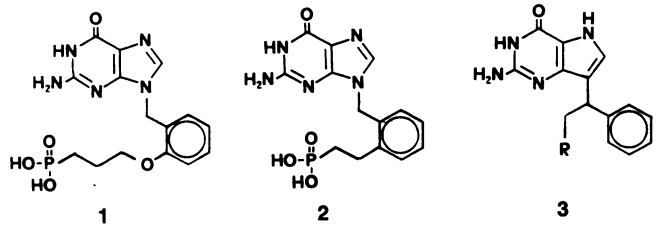

Subsequent crystallographic analysis revealed that the plane of the aromatic ring had rotated ≈90° in order to accommodate the long spacer. More sophisticated modeling studies using coordinates from the guanine–PNP complex and Monte Carlo/energy minimization techniques predicted that a two-carbon spacer would provide a better fit while maintaining the optimum orientation of the aromatic ring. A compound (structure 2) with a two-carbon spacer was a much better inhibitor of PNP; however, it was clear from the x-ray analysis that the aromatic ring was still not able to form an ideal Herringbone packing interaction. Concurrently, compounds (structure 3) were being modeled in which the spacer to the phosphate binding site branched from the benzylic carbon, thus placing no direct restrictions on the tilt of the aromatic ring. Several compounds have now been prepared in this series and confirm the modeling studies based on the x-ray structure. One of the racemic mixtures was separated, individual IC_{50} values were determined, and crystallographic analysis was carried out on the enantiomers. This analysis showed that the *S* isomer is the potent PNP inhibitor. Fig. 6 shows an active site model of the best PNP inhibitor along with the experimental electron density. This series of compounds contains the most potent membrane-permeable inhibitors of PNP yet reported.‖

Summary. Crystallographic and modeling methods have been combined with organic synthesis to produce inhibitors

‖A variety of *in vivo* assays have been performed for the most potent PNP inhibitors. These include evaluation of T-cell cytotoxicity in cell cultures and elevation of inosine levels resulting from PNP inhibition in rats.

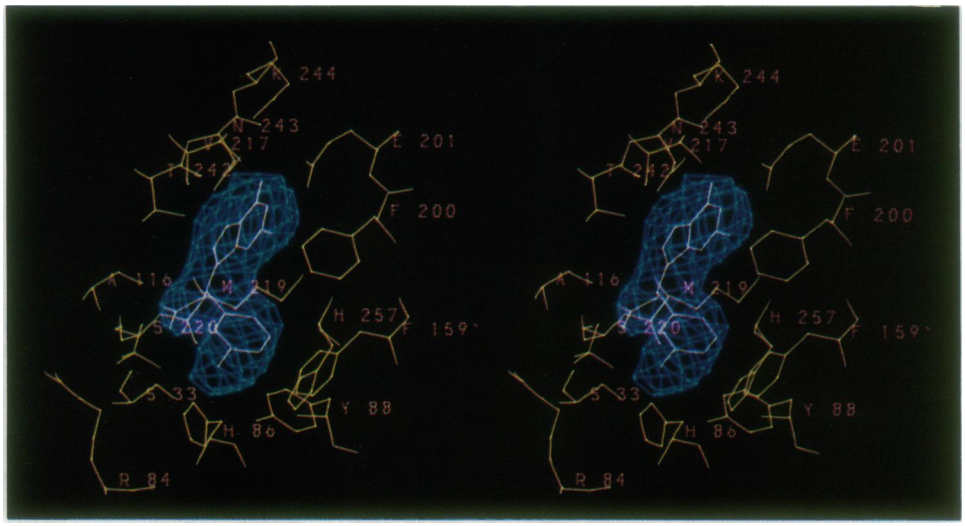

FIG. 6. Binding geometry of the best PNP inhibitor (Table 1, first entry). The difference electron density (complex native) at 3.2 Å resolution is shown for the inhibitor. The key amino acid residues in the active site are shown. The phosphate ion, which would normally be displaced by the inhibitor, is also shown for reference.

of PNP. Kinetic data for selected compounds showed that the inhibitors are competitive with respect to inosine. The approach can best be described as iterative, in which accumulated knowledge is used to produce optimized compounds. Competitive inhibitors benefit from the following features: (*i*) an analog purine base with hydrogen bonds to Glu-201, Thr-242, Asn-243, and/or Lys-244, (*ii*) a bulky hydrophobic group near the ribose binding site, (*iii*) a substituent with affinity for the phosphate binding site, and (*iv*) spacers that link these groups together without perturbing the binding geometry of the individual groups. These features are exemplified in compounds such as (*S*)-9-[1-(3-chlorophenyl)-2-carboxyethyl]-9-deazaguanine (Table 1, first entry), which exhibits an IC_{50} value of 5.9 nM.

We found that computer modeling required significant tuning in order to provide useful results. Crystallographic results were useful in testing and modifying modeling parameters. The most useful modeling results were achieved after incorporation of the conformational searching techniques described above and when the coordinates for the PNP–guanine complex model were used.

Crystallographic analysis was based primarily on the results of difference Fourier maps in which the quantitative relationships between residues in the active site and the inhibitor could be characterized. During these studies, ≈35 PNP–inhibitor complexes were evaluated by x-ray crystallographic techniques. It is noteworthy that the resolution of the PNP model extends to only 2.8 Å and that all of the difference Fourier maps were calculated at 3.2 Å resolution, much lower than often considered essential for drug design. Crystallographic analysis was facilitated by the large solvent content that allowed for free diffusion of inhibitors into enzymatically active crystals (28). During the 2.5 years of this project, ≈60 active compounds were synthesized. The large number of active compounds designed and the enhancement in inhibitor potency of nearly 2 orders of magnitude stand as proof that crystallographic and computer-assisted modeling methods are now capable of playing a critical role in the rapid discovery of therapeutic agents.

We thank Dr. S. Narayana, Dr. W. Cook, Dr. M. Carson, and Mrs. C. Woodruff of the University of Alabama at Birmingham; Drs. S. Niwas, R. Elliot, J. Rose, S. Ananthan, L. Bennett, and P. Allen of the Southern Research Institute; Drs. M. Allen, F. Clarke, and J. Stanton of CIBA–Geigy; Drs. J. Stoeckler and R. Parks, Jr., of Brown University; Drs. J. Tuttle and T. Krenitsky of Burroughs Wellcome. This research was supported by grants from the American Cancer Society (CH-213), the Leukemia Society of America, the National Institutes of Health (GM-38823), and the National Aeronautics and Space Administration (NAGW-813 and NAS8-36611).

1. Erickson, J., Neidhart, D. J., VanDrie, J., Kempf, D. J., Wang, X. C., Norbeck, D. W., Plattner, J. J., Rittenhouse, J. W., Turon, M., Wideburg, N., Köhlbrenner, W. E., Simmer, R., Helfrich, R., Paul, D. A. & Knigge, M. (1990) *Science* **249**, 527–533.
2. McCammon, J. A. & Harvey, S. C. (1987) *Dynamics of Proteins and Nucleic Acids* (Cambridge Univ., New York).
3. Van Gunsteren, W. F. & Weiner, P. K., eds. (1989) *Computer Simulation of Biomolecular Systems: Theoretical and Experimental Applications* (Escom Science, Leiden, The Netherlands).
4. Stoeckler, J. D. (1984) in *Developments in Cancer Chemotherapy*, ed. Glazer, R. E. (CRC, Boca Raton, FL), pp. 35–60.
5. Friedkin, M. & Kalckar, H. (1961) in *The Enzymes*, eds. Boyer, P. D., Lardy, H. & Myrback, K. (Academic, New York), 2nd Ed., Vol. 5, pp. 237–255.
6. Parks, R. E., Jr., & Agarwal, R. P. (1972) in *The Enzymes*, ed. Boyer, P. D. (Academic, New York), 3rd Ed., Vol. 7, pp. 483–514.
7. Agarwal, K. C., Agarwal, R. P., Stoeckler, J. D. & Parks, R. E., Jr. (1975) *Biochemistry* **14**, 79–84.
8. Bzowska, A., Kulikowska, E. & Shugar, D. (1990) *Z. Naturforsch. C: Biosci.* **45**, 59–70.
9. Stoeckler, J. D., Agarwal, R. P., Agarwal, K. C., Schmid, K. & Parks, R. E., Jr. (1978) *Biochemistry* **17**, 278–283.
10. Williams, S. R., Goddard, J. M. & Martin, D. W., Jr. (1984) *Nucleic Acids Res.* **12**, 5779–5787.
11. LePage, G. A., Junga, I. G. & Bowman, B. (1964) *Cancer Res.* **24**, 835–840.
12. Erion, M. D. (1990) *Eur. Patent Appl.* 374,096.
13. Giblett, E. R., Ammann, A. J., Wara, D. W., Sandman, R. & Diamond, L. K. (1975) *Lancet* **i**, 1010–1013.
14. Sircar, J. C. & Gilbertsen, R. B. (1988) *Drugs of the Future* **13**, 653–668.
15. Stoeckler, J. D., Ealick, S. E., Bugg, C. E. & Parks, R. E., Jr. (1986) *Fed. Proc. Fed. Am. Soc. Exp. Biol.* **45**, 2773–2778.
16. Ealick, S. E., Rule, S. A., Carter, D. C., Greenhough, T. J., Babu, Y. S., Cook, W. J., Habash, J., Helliwell, J. R., Stoeckler, J. D., Parks, R. E., Jr., Chen, S.-F. & Bugg, C. E. (1990) *J. Biol. Chem.* **265**, 1812–1820.
17. Mohamadi, F., Richards, N. G. J., Guida, W. C., Liskamp, R., Lipton, M., Caufield, C., Change, G., Hendrickson, T. & Still, W. C. (1990) *J. Comput. Chem.* **11**, 440–467.
18. Weiner, S. J., Kollman, P. A., Case, D. A., Singh, U. C., Ghio, C., Alagona, S., Profeta, S. & Weiner, P. (1984) *J. Am. Chem. Soc.* **106**, 765–784.
19. Weiner, S. J., Kollman, P. A., Nguyen, T. D. & Case, D. A. (1986) *J. Comput. Chem.* **7**, 230–252.
20. Chang, G., Guida, W. C. & Still, W. C. (1989) *J. Am. Chem. Soc.* **111**, 4379–4386.
21. Stoeckler, J. D., Cambor, C., Kuhns, V., Chu, S.-H. & Parks, R. E., Jr. (1982) *Biochem. Pharmacol.* **31**, 163–171.
22. Shewach, D. S., Chern, J.-W., Pillote, K. E., Townsend, L. B. & Daddona, P. E. (1986) *Cancer Res.* **46**, 519–523.
23. Stoeckler, J. D., Ryden, J. B., Parks, R. E., Jr., Chu, M.-Y., Lim, M.-I., Ren, W.-Y. & Klein, R. S. (1986) *Cancer Res.* **46**, 1774–1778.
24. Tuttle, J. V. & Krenitsky, T. A. (1984) *J. Biol. Chem.* **259**, 4065–4069.
25. Gilbertsen, R. B., Scott, M. E., Dong, M. K., Kossarek, L. M., Bennett, M. K., Schrier, D. J. & Sircar, J. C. (1987) *Agents Actions* **21**, 272–274.
26. Burley, S. K. & Petsko, G. A. (1985) *Science* **229**, 23–28.
27. Castleman, B. & McNeely, B. U., eds. (1974) *N. Engl. J. Med.* **290**, 39–49. 653.
28. Ealick, S. E., Babu, Y. S., Narayana, S. V. L., Cook, W. J. & Bugg, C. E. (1990) in *Advances in Chemotherapy of AIDS*, eds. Diasio, R. B. & Sommadossi, J.-P. (Pergamon, New York), pp. 97–108.
29. Appelt, K., Bacquet, R. J., Bartlett, C. A., Booth, C. L. J., Freer, S. T. *et al.* (1991) *J. Med. Chem.* **34**, 1925–1934.